LAWRENCE
LIVERMORE
NATIONAL
LABORATORY

LLNL-CONF-767121

Autoignition experiments and kinetic modeling of selected highly-branched C8-C16 iso-alkanes for surrogate fuel applications

R. Fang, G. Kukkadapu, M. Wang, S. W. Wagnon, K. Zhang, M. Mehl, C. K. Westbrook, W. J. PITZ, C. J. Sung

February 1, 2019

11Th US National Combustion meeting
Pasedena, CA, United States
March 24, 2019 through March 27, 2019

Disclaimer

11th U.S. National Combustion Meeting
Organized by the Western States Section of the Combustion Institute
March 24-27, 2019
Caltech, Pasadena

Autoignition experiments and kinetic modeling of selected highly-branched C_8–C_{16} *iso*-alkanes for surrogate fuel applications

Ruozhou Fang[1], Goutham Kukkadapu[2], Mengyuan Wang[1,2], Scott W. Wagnon[2], Kuiwen Zhang[2], Marco Mehl[2], Charles K. Westbrook[2], William J. Pitz[2], Chih-Jen Sung[1]*

[1]Department of Mechanical Engineering, University of Connecticut, Storrs, CT, USA
[2]Lawrence Livermore National Laboratory, Livermore, CA, USA
**Corresponding Author: ruozhou.fang@uconn.edu*

Abstract: Highly-branched *iso*-alkanes are an important class of hydrocarbons found in conventional petroleum-derived and alternative renewable fuels used for combustion applications. However, chemical kinetics for most of these *iso*-alkanes, especially at low-to-intermediate temperatures, have not been well studied. Recognizing this, autoignition of selected *iso*-alkanes, including *iso*-octane (2,2,4-trimethylpentane), *iso*-nonane (2,2,4,4-tetramethylpentane), *iso*-dodecane (2,2,4,6,6-pentamethylheptane), and *iso*-cetane (2,2,4,4,6,8,8 heptamethylnonane), has been investigated both experimentally and numerically in this study. Experiments using a rapid compression machine have been conducted to understand and compare the ignition characteristics of these *iso*-alkanes at varying pressures, temperatures, equivalence ratios, and dilution levels. By comparing their experimental pressure traces and ignition delay times, the fuel molecular structure effect on autoignition under low temperature combustion conditions for these highly-branched *iso*-alkanes are demonstrated and discussed. Furthermore, a newly-developed chemical kinetic model covering C_8–C_{16} *iso*-alkanes is detailed herein. Simulated results using this model are then compared to the experimental data obtained in this study and available in the literature. The ability of the current chemical kinetic model to predict the experimental trends is illustrated. Chemical kinetic analyses have also been conducted to identify the important reaction pathways controlling autoignition at varying conditions.

Keywords: ***iso-alkane, autoignition, rapid compression machine, low temperature combustion, chemical kinetics***

1. Introduction

As fuel surrogates containing only a few representative components are used to emulate the physical and chemical characteristics of the target real fuels, understanding the combustion characteristics of those pure components can greatly benefit the development of comprehensive surrogate models for simulating real fuel combustion [1]. Among various representative fuel components found in conventional and alternative transportation fuels, highly-branched *iso*-alkanes are one important hydrocarbon class and plays a significant role in the autoignition properties of the real fuels. As such, previous studies extensively investigated the autoignition characteristics of *iso*-octane (2,2,4-trimethylpentane, iC8) at low-to-high temperatures [2-22] and *iso*-cetane (2,2,4,4,6,8,8-heptamethylnonane, iC16) at low-to-high

temperatures [4,23-26]. While limited autoignition data for *iso*-dodecane (2,2,4,6,6-pentamethylheptane, iC12) were reported in [4,27], autoignition of *iso*-nonane (2,2,4,4-tetramethylpentane, iC9) has not been studied yet. It is also noted that for most of *iso*-alkanes, their autoignition chemistry at low-to-intermediate temperatures has not been well understood. In view of the above, developing a comprehensive chemical kinetic model that covers *iso*-alkanes from C_8 to C_{16} with low-to-intermediate temperature chemistry, as well as providing model validation datasets of iC9 and iC12 over a wide range of conditions, are of fundamental importance.

In this investigation, a rapid compression machine (RCM) is used to measure ignition delay times of iC8/air, iC9/air, and iC12/air mixtures at varying pressures (15, 20, and 30 bar), equivalence ratios (0.7, 1.0, 1.2, and 2.0), and temperatures (600–900 K). The current RCM measurements are compared with the previous RCM data of iC8 [2] and the shock tube (ST) data of iC8 [3] and iC12 [4], demonstrating the consistency of the current RCM data and the literature RCM/ST data. In addition, the present experimental data of iC8, iC9, and iC12 are compared with the RCM data of iC16 reported in [23,24] to understand the fuel molecular structure effect on autoignition under low temperature combustion relevant conditions. Figure 1 shows the molecular structures of the *iso*-alkanes investigated in this study. A detailed chemical kinetic model, including low-to-high temperature chemistry, for *iso*-alkanes is also developed. The performance of this chemical kinetic model is validated against the newly-acquired RCM measurements and the literature data. Furthermore, model-based sensitivity analysis is performed to identify the key reaction pathways controlling the autoignition of the *iso*-alkanes studied herein.

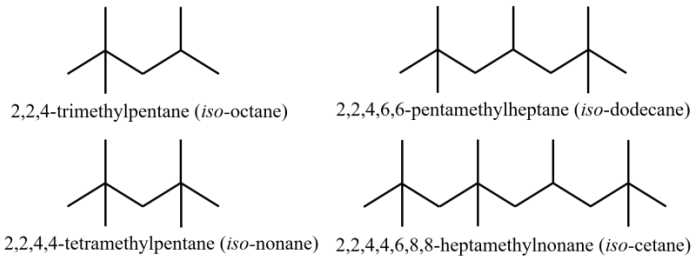

Figure 1: Molecule structures of *iso*-octane, *iso*-nonane, *iso*-dodecane, and *iso*-cetane.

2. Experimental Specifications

The RCM used in this study is a single piston arrangement and is pneumatically driven and hydraulically stopped. The device has been described in detail previously [28,29] and will be described here briefly for reference. The end of compression (EOC) temperature and pressure, T_C and P_C, respectively, are independently changed by varying the overall compression ratio, initial pressure, and initial temperature of each experiment. The primary diagnostic on the RCM is the in-cylinder dynamic pressure which is measured using a shock-resistant Kistler 6125C pressure transducer. The raw pressure data is processed by a Python package called UConnRCMPy [30], which determines P_C, T_C, and ignition delay time(s). Figure 2(a) shows the non-reactive and reactive experimental pressure traces obtained by the RCM and the definitions of the first-stage ignition delay (τ_1) and the total ignition delay (τ). Namely, τ_1 and τ are defined as the time from the EOC to the respective maximum of the first order time derivative of pressure (dP/dt). In addition, to determine the machine-specific effect (i.e., the heat loss effect [31]) on the reactive experiment and to confirm that there is no exothermicity during the compression stroke, the corresponding non-reactive experiment is also conducted by replacing O_2 in the reactive mixture with N_2.

It is shown in Fig. 2(a) that the pressure trace of the reactive experiment during the compression stroke and prior to the first-stage ignition after reaching the EOC is well captured by the non-reactive counterpart. Moreover, heat loss during or after the compression stroke is modeled here as changing the volume of the reaction chamber [28,32].

At least four consecutive runs were taken for each experimental condition to ensure repeatability, as shown in Fig. 2(b). Among repeated experiments, the one with τ closest to the averaged value is selected as the representative pressure trace. The associated parameters (such as P_C and T_C) and outputs (such as τ and τ_1) of each representative experiment are reported instead of reporting all repeated experiments. The typical scatters of τ_1 and τ for repeated experiments are less than 15% of the reported values.

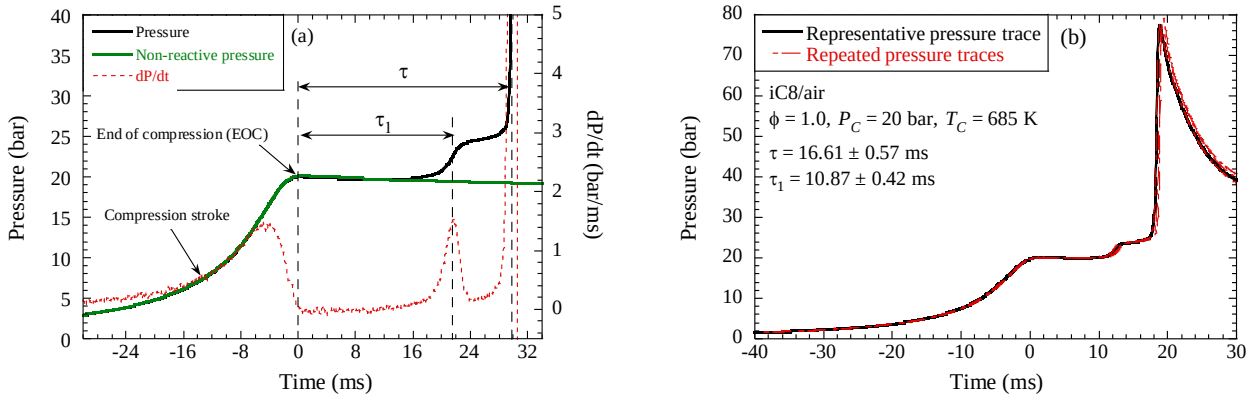

Figure 2: (a) Example experimental pressure traces demonstrating the definitions of the τ_1 and τ with iC12/air at ϕ=1.0, P_C=20 bar, and T_C=647 K. (b) Representative and repeated experimental pressure traces with iC8/air at ϕ=1.0, P_C=20 bar, and T_C=685 K.

Table 1. Summary of test conditions and literature data

Fuel type	Equivalence ratio, ϕ	P_C (bar)	Molar proportions (%)			Temperature regime covered
			Fuel	O_2	N_2	
iC8	0.7	20	1.1628	20.7641	78.0731	ITR/NTC/LTR
	1.0	15,20,30	1.6529	20.6612	77.6859	ITR/NTC/LTR
	2.0	20	3.2520	20.3252	76.4228	NTC/LTR
iC9	0.7	20	1.0395	20.7900	78.1705	ITR/NTC/LTR
	1.0	15,20,30	1.4784	20.6978	77.8238	ITR/NTC/LTR
	1.2	20	1.7689	20.6368	77.5943	ITR/NTC/LTR
	2.0	20	2.9137	20.3963	76.6900	ITR/NTC/LTR
iC12	0.7	20	0.7886	20.8427	78.3687	ITR/NTC/LTR
	1.0	15,20,30	1.1228	20.7725	78.1047	ITR/NTC/LTR
	2.0	20	2.2207	20.5419	77.2374	ITR/NTC/LTR
iC16 (literature)	1.0	15,20 [23]	0.8502	20.8298	78.3200	ITR/NTC
	1.0	15 [24]	0.8502	20.8298	78.3200	ITR

The fuel-oxidizer mixture is prepared in a pre-vacuumed stainless-steel mixing tank at room temperature. A known amount of liquid fuel is injected into the mixing tank first. Then, O_2 and N_2 are filled into the mixing tank consecutively based on barometric measurements. After filling the reactants,

the heaters and magnetic stirrer are switched on, and the system is allowed for 4 hours to reach steady state. The molar ratio of N_2 and O_2 is kept at 3.76 throughout this study. Table 1 summarizes the molar proportions of the test mixtures and the corresponding test conditions investigated herein, along with those studied in [23,24] for iC16. Most of the test conditions covered the low temperature regime (LTR), the negative temperature coefficient (NTC) regime, and the intermediate temperature regime (ITR).

3. Computational Specifications

3.1. Chemical kinetic model for *iso*-alkanes

The detailed chemical kinetic model of *iso*-alkanes developed in this study enclosed the sub-models of iC8 and iC12. This is a portion of the full model [33] that includes iC8, iC9, iC12, and iC16 sub-models. The model of iC8 and iC12 is built hierarchically on the model of Zhang et al. [34] for alkanes and the C_0–C_4 base chemistry of AramcoMech 2.0 [35]. Briefly, the current model describes both the high temperature and low temperature kinetics of iC8 and iC12 using a consistent set of reaction pathways and the associated reaction rates. The reaction rates for the high temperature reaction classes 1–9, as described by Curran et al. [36], have largely been taken from the earlier work of Mehl et al. [37], with an exception to H-abstraction via $\dot{O}H$ which was taken from the work of Badra and Farooq [38]. The rates for the low temperature reaction classes 10–25, as described by Curran et al. [36], which are the low temperature chain branching peroxy reactions, have been adopted from the ab-initio works of [39-42]. In addition to the above-mentioned 25 classes, the reaction classes corresponding to the concerted elimination of alkyl peroxy radicals (commonly referred as $\dot{R}O_2$ radicals) and hydroperoxyl alkylhydroperoxides (commonly referred as $\dot{O}OQOOH$ radicals), as well as the alternative isomerization reactions of $\dot{O}OQOOH$ radicals producing the dihydroperoxy alkyl radicals (commonly referred as $\dot{P}(OOH)_2$ radicals), have also been modeled. Those additional low temperature reaction pathways are for revising the details of the chain branching, chain propagation, and chain termination functions in the model. It is necessary to point out that the reaction pathways of $\dot{P}(OOH)_2$ is largely based on analogies from $\dot{Q}OOH$. As the isomerization reaction of $\dot{O}OQOOH \Leftrightarrow \dot{P}(OOH)_2$ is similar to $\dot{R}O_2 \Leftrightarrow \dot{Q}OOH$, analogies from the latter are adapted to describe the formation of $\dot{P}(OOH)_2$. Likewise, as the $\dot{P}(OOH)_2$ and $\dot{Q}OOH$ radicals are similar in nature, the $\dot{P}(OOH)_2$ radicals have been modeled to undergo reactions identical to those of $\dot{Q}OOH$ radicals and analogies are used for describing the reactions of $\dot{P}(OOH)_2$ radicals. The important low temperature reaction classes and their sources are summarized in Table 2.

The thermodynamic properties of the intermediate species have been estimated using the group additivity method with the recent group values taken from Burke et al. [43]. As the *iso*-alkanes studied herein are severely branched, the Gauche interactions and H-1,5 interactions were also counted during the estimation of the thermodynamic properties. The procedure used for counting those interactions is similar to that used in the study of Atef et al. [2].

Table 2. Important low temperature reaction classes and the corrospond sources

Reaction Class	Source
$\dot{R} + O_2 \Leftrightarrow \dot{R}O_2$	Miyoshi [39]
$\dot{R}O_2 \Leftrightarrow \dot{Q}OOH$	Villano et al. [40]
Concerted elimination of $\dot{R}O_2$ and $\dot{O}OQOOH$	Villano et al. [40]
$\dot{Q}OOH \Leftrightarrow \text{Cyclic ethers} + OH$	Miyoshi [39], Villano et al. [41]
$\beta\text{-}\dot{Q}OOH \Leftrightarrow H\dot{O}_2 + \text{olefin}$	Villano et al. [41]
$\dot{Q}OOH + O_2 \Leftrightarrow \dot{O}OQOOH$	Miyoshi [39]
$\dot{O}OQOOH \Leftrightarrow \text{Ketohydroperoxides (KHP)} + \dot{O}H$	Sharma et al. [42]
$\dot{O}OQOOH \Leftrightarrow \dot{P}(OOH)_2$	Villano et al. [40]
Decomposition of $\dot{Q}OOH$ and $\dot{P}(OOH)_2$	Villano et al. [41]
$\dot{P}(OOH)_2 \Leftrightarrow HPCE + \dot{O}H$	Miyoshi [39], Villano et al. [41]

3.2. Simulation methods

Two types of simulations are performed using the Python interface of Cantera 2.3.0 [44] in this study. The first type is 'RCM simulation' [45] that accounts for the machine-specific effect by modeling it as volume change. A volume trace is deduced using the corresponding non-reactive pressure trace by assuming that the constant-composition mixture undergoes an isentropic compression during the compression stroke and an isentropic expansion after the EOC. The volume trace is then fed to the `IdealGasReactor` in Cantera to generate a simulated reactive pressure trace, from which the τ_1 and τ values of RCM simulation are obtained following the same procedure of determining experimental ignition delays described in Section 2.

The second type of simulation is 'CONV simulation' that uses a constant-volume, adiabatic reactor, which is the `IdealGasReactor` in Cantera without accounting for changes in the reactor volume. The simulated τ values are defined as the time required for the simulated temperature to increase by 400 K over the initial temperature in the simulation. The CONV simulations in this study are mainly used to perform ST simulations and model-based analyses. The non-ideal facility-dependent effects of ST simulation [46,47] are not considered in this work.

3.3. Sensitivity analysis

To identify the dominating reaction pathways in each *iso*-alkane's autoignition process, model-based sensitivity analyses for τ to the pre-exponential factor of each reaction rate are performed utilizing CONV simulations in Cantera with the current chemical kinetic model. By perturbing the pre-exponential factor of the target reaction by a factor of 2 or 0.5, the corresponding τ values are simulated and recorded. The sensitivity coefficient is defined as $S_\tau = \ln(\tau^+/\tau^-)/\ln(2/0.5)$, where τ^+ and τ^- are the total ignition delays when the pre-exponential factor modification equal to a factor of 2 and 0.5,

respectively. From this analysis, the reactions that promote (inhibit) the reactivity exhibit a negative (positive) sensitivity coefficient.

4. Results and Discussion

4.1. Comparison with literature data

Figure 3 compares the total ignition delays of stoichiometric iC8/air and iC12/air mixtures at 20 bar obtained from the current RCM experiments to the literature RCM data of iC8 [2] and the ST data reported in [3] and [4] for iC8 and iC12, respectively. Overall, the current RCM measurements complement well with the literature ST data, illustrating the importance of the new RCM datasets for model validation at low-to-intermediate temperatures, for the case of iC12 in particular. Regarding the RCM data comparison for iC8, while small discrepancies in the LTR and the NTC regime are noticed between the previous and current measurements, the newly-acquired τ and τ_1 of iC8 generally match well with those reported in [2], especially considering varying heat loss characteristics and initial temperature/pressure conditions in different RCM experiments. Using the chemical kinetic model developed in this study, the RCM and ST data are modeled using 'RCM simulation' and 'CONV simulation', respectively. Figure 3 shows that the simulated results agree well with the experimental τ and τ_1 of iC8 and iC12, illustrating the predicting capability of the current model over a wide range of temperatures. It has to be pointed out in both iC8 and iC12 cases that 'CONV simulation' slightly over-predicts the literature ST data. These discrepancies are likely induced by the non-ideal, facility-dependent effects in the shock tube experiments. Including the facility-dependent effects in ST simulations is expected to improve the agreement between simulated and experimental results.

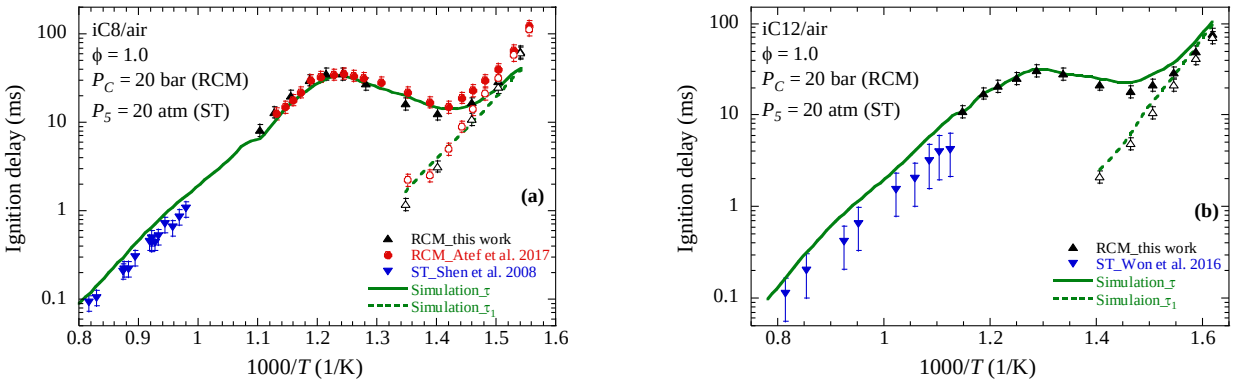

Figure 3: Comparison of ignition delay times of stoichiometric (a) iC8/air and (b) iC12/air mixtures between the current RCM study and the literature RCM and shock tube (ST) data. Experimental results are shown as symbols. Filled symbols: total ignition delay times. Open symbols: first-stage ignition delay times. Simulated results are presented as lines. Solid line: total ignition delay times; dashed line: first-stage ignition delay times.

4.2. Autoignition characteristics of selected *iso*-alkanes

Figure 4 demonstrates the pressure trace comparison for stoichiometric iC8/air, iC9/air, and iC12/air mixtures at P_C=15 bar with three representative temperatures of T_C ~ 645 K, 745 K, and 837 K, covering the LTR, NTC regime, and ITR, respectively. All three *iso*-alkanes exhibit two-stage ignition behavior at LTR, as shown in Fig. 4 (a). In the NTC regime for T_C~745 K, Fig. 4(b) shows that iC8 exhibits a two-stage ignition behavior with very short τ_1, while both iC9 and iC12 display single-stage ignition

behavior. Further increasing T_C to 837 K (ITR), all three *iso*-alkanes exhibit single-stage ignition behavior, as illustrated in Fig. 4(c). While iC9 consistently exhibits the shortest τ compared to iC8 and iC12 among all tested temperatures, a clear reactivity crossover between iC8 and iC12 is observed as temperature increases from the LTR to the ITR. Namely, iC8 has shorter τ than iC12 in NTC regime, but becomes longer in the LTR and ITR. This reactivity crossover will be discussed in detail in Section 4.3. It is also noted that for all three fuels shown in Fig. 4(a), their machine settings in RCM experiments are similar. As the values of heat of combustion on a unit mass of fuel basis are similar for iC8/iC9/iC12, their peak pressures after hot-ignition are similar (~64 bar). Furthermore, it has to be pointed out that the observed differences in the post-hot-ignition peak pressure values among iC8, iC9, and iC12 in Figs. 4(b) and 4(c) are caused by the different machine settings used in RCM experiments to achieve the desired compressed conditions for each fuel.

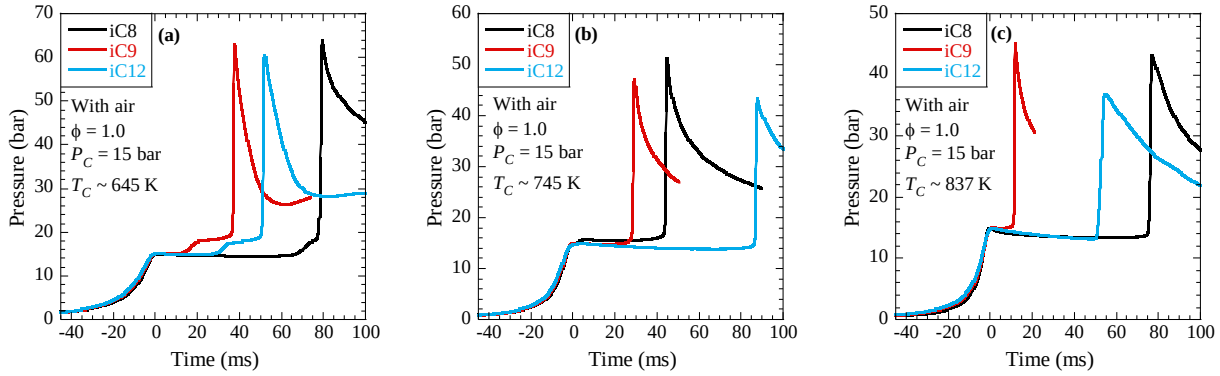

Figure 4: Pressure trace comparison of stoichiometric iC8/air, iC9/air, and iC12/air mixtures at P_C=15 bar and three different compressed temperatures of (a) T_C~645 K (LTR), (b) T_C~745K (NTC), and (c) T_C~837 K (ITR).

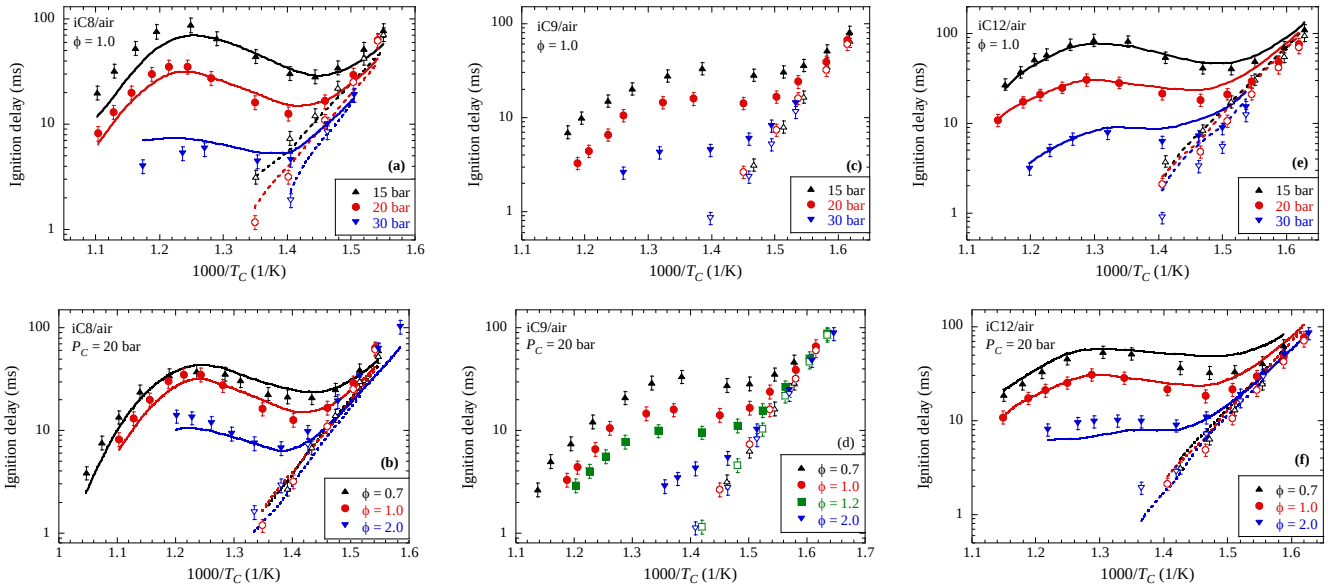

Figure 5: Experimental and simulated ignition delay times of iC8, iC9, and iC12 at varying ϕ and P_C. (a) iC8, ϕ=1.0, and varying P_C; (b) iC8, P_C=20 bar, and varying ϕ; (c) iC9, ϕ=1.0, and varying P_C; (d) iC9, P_C=20 bar, and varying ϕ; (e) iC12, ϕ=1.0, and varying P_C; (f) iC12, P_C=20 bar, and varying ϕ. Experimental results are shown as symbols. Filled symbols: total ignition delay times. Open symbols:

first-stage ignition delay times. Simulated results are presented as lines. Solid lines: total ignition delay times. Dashed lines: first-stage ignition delay times.

Figure 5 shows the measured τ_1 and τ for the iC8/air, iC9/air, and iC12/air mixtures investigated. Among all three *iso*-alkanes at various test conditions, τ decreases with increasing T_C in the LTR and ITR, while it increases with increasing T_C in the NTC regime. On the other hand, τ_1 decreases monotonically with increasing T_C. The magnitude of NTC response, reflected by the slope in the Arrhenius plot, is also different among three *iso*-alkanes; iC8 shows the strongest NTC response while iC9 exhibits the weakest one at the same conditions of P_C and ϕ. In addition, Figs. 5(a), 5(c), and 5(e) demonstrate the effect of pressure on ignition delay times of stoichiometric iC8, iC9, and iC12 mixtures in air, respectively. In general, both τ_1 and τ decrease with increasing P_C, with τ showing stronger pressure sensitivity than τ_1. It is further noted that the NTC response becomes weaker when increasing P_C to 30 bar for all three fuels. Moreover, unlike the other two *iso*-alkanes, the τ_1 of iC9 is nearly insensitive to pressure change. At P_C=20 bar, Figs. 5(b), 5(d), and 5(f) show the effect of equivalence ratio on ignition delay times for iC8, iC9, and iC12, respectively. Since "air" is used as the oxidizer here, the effect of equivalence ratio represents the effect of fuel loading. In general, for all three *iso*-alkanes, increasing ϕ (i.e. fuel concentration) decreases τ for a given T_C, while τ_1 is far less sensitive to the change in ϕ as compared to τ.

Using the current chemical kinetic model, RCM simulations of iC8 and iC12 are conducted at various conditions. Overall, the simulated results of τ_1 and τ show good agreement against experimental data at varying P_C and ϕ for both iC8 and iC12. Nonetheless, some discrepancies are still noticed at a few test conditions. For iC8 in the ITR, the current model under-predicts τ at P_C=15 and 20 bar but over-predicts τ at P_C=30 bar, as shown in Fig. 5(a). For iC12, the simulated τ_1 and τ in the LTR are slightly longer than the RCM data, especially at P_C=30 bar as shown in Fig. 5(e). These observations suggest that pressure dependency of some low-to-intermediate temperature reactions in the model may require refinements. Despite the above-mentioned discrepancies, the performance of the current model is sound, illustrating its predicting capability as well as its potential of being used in understanding the autoignition characteristics of *iso*-alkanes.

4.3. Comparison of iC8, iC9, iC12, and iC16

To provide an insight into the differences and similarities between the selected *iso*-alkanes at low-to-intermediate temperatures, Figs. 6 and 7 compare the newly-acquired ignition delay data of iC8/air, iC9/air, and iC12/air mixtures at varying test conditions. Moreover, the literature RCM data of stoichiometric iC16/air mixtures at P_C=15 bar [23,24] and 20 bar [23] are also included in Fig. 6 for comparison. It needs to be pointed out that some discrepancies between the two literature iC16 datasets are noted in Fig. 6, which can be attributed to the differences in heat loss characteristics in the respective RCM experiments. Thus, the effects of heat loss among different RCMs need to be considered when comparing and discussing the current iC8/iC9/iC12 results and the literature iC16 data.

As presented in Fig. 6 (comparison including iC16 data) and Fig. 7 (comparison without iC16 data), the four *iso*-alkanes exhibit distinct autoignition characteristics. First, iC9 and iC8 exhibits the weakest and strongest NTC response, respectively. Second, the temperature windows of the NTC regime are different among the four *iso*-alkanes, with those of iC8 and iC12 being situated at higher temperatures

relative to that of iC16. In addition, the NTC temperature window of iC9 is much narrower than those of the other three *iso*-alkanes.

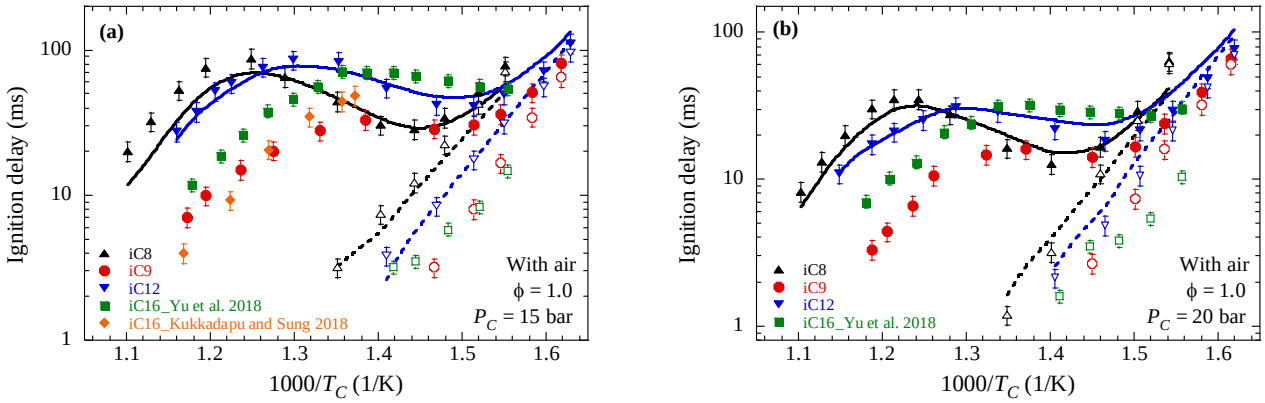

Figure 6: Experimental and simulated ignition delay times of stoichiometric iC8/air, iC9/air, iC12/air, and iC16/air mixtures at (a) P_C=15 bar and (b) P_C=20 bar. Experimental results are shown as symbols. Filled symbols: total ignition delay times. Open symbols: first-stage ignition delay times. Simulated results are presented as lines. Solid lines: total ignition delay times; dashed lines: first-stage ignition delay times.

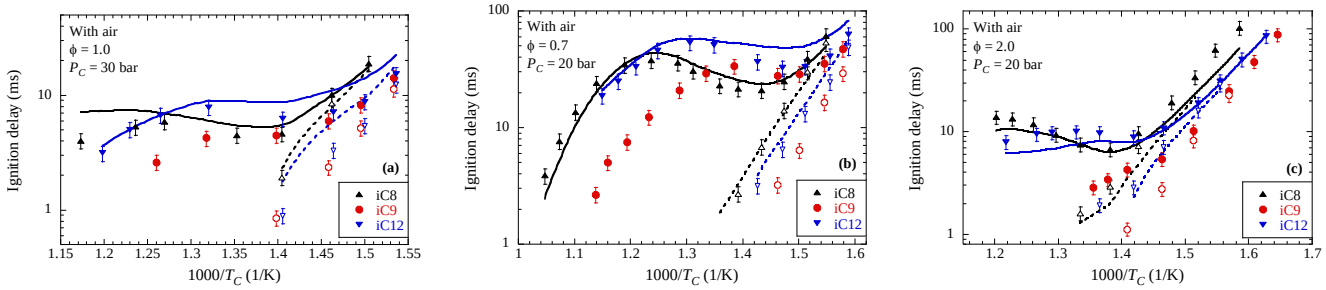

Figure 7: Experimental and simulated ignition delay times of iC8/air, iC9/air, and iC12/air mixtures at different compressed pressures and equivalence ratios. (a) P_C=30 bar and ϕ=1.0, (b) P_C=20 bar and ϕ=0.7, and (c) P_C=20 bar and ϕ=2.0. Experimental results are shown as symbols. Filled symbols: total ignition delay times. Open symbols: first-stage ignition delay times. Simulated results are presented as lines. Solid lines: total ignition delay times; dashed lines: first-stage ignition delay times.

Based on Figs. 6 and 7, the reactivity of each *iso*-alkane is examined at various test conditions. For ϕ ≥1, the most reactive *iso*-alkane is iC9 as it exhibits the shortest τ. When ϕ<1, the τ of iC9 in the NTC regime becomes longer than those of iC8 as shown in Fig. 7(b). Comparing iC8 and iC12, the τ of iC8 is consistently longer than that of iC12 in the LTR/ITR; however, in NTC regime the τ of iC8 becomes shorter than that of iC12. This indicates that there is a reactivity crossover between iC8 and iC12 over different temperature regimes. The similar reactivity crossover is also observed among iC8, iC12, and iC16 as seen in Fig. 6. In the NTC regime, the τ of iC16 is longer than those of iC8 and iC12. However, the τ of iC16 in the ITR is the shortest compared to those of iC8 and iC12. As all experiments of iC8, iC9, and iC12 in this study were performed using the same RCM, their heat loss profiles are similar at the same test condition (ϕ, T_C, P_C). Thus, the observed reactivity crossover is not affected by different heat loss characteristics among three *iso*-alkanes. Comparing the simulated τ between iC8 and iC12, the experimentally observed reactivity crossover is successfully captured by the current model at various

test conditions. This further substantiates the potential of the current model as a tool to understand the autoignition of iC8 and iC12 at low temperatures.

It is of interest to note that the above-mentioned reactivity crossovers among *iso*-alkanes are not observed in the comparison among *n*-alkanes [48]. The total ignition delay times of *n*-alkanes are shown to slightly decrease with increasing carbon number over a wide range of temperatures due to the lower carbon-carbon bond energy for larger *n*-alkanes [48]. For *iso*-alkanes, however, the bond energy theory alone cannot explain the reactivity crossover observed in the low-to-intermediate temperature regime. Therefore, the uniqueness of the molecular structure for each *iso*-alkane may lead to different reactivity trends among them.

Another interesting observation from Figs. 6 and 7 is that the experimental τ of iC9 and iC12 in the LTR overlap well at all test conditions except for the ϕ=2.0 case, while iC8 has different τ in the LTR as compared to iC9 and iC12. On the other hand, the experimental τ_1 comparison among the four *iso*-alkanes shows a more consistent trend. At all test conditions, the τ_1 ranking generally follows iC9<iC12<iC8, and the slopes of τ_1 in the Arrhenius plots are very close among them. However, iC16 exhibits a gentler τ_1 slope compared to iC8/iC9/iC12, and hence crosses with iC9 as shown in Fig. 6. This could be attributed to the different heat loss characteristics between the RCMs used in this work and in Yu et al. [23]. Moreover, the simulated results of τ_1 well capture the experimental τ_1 ranking of iC8 and iC12 at various test conditions.

4.4 Model-based sensitivity analysis

As a work in progress, preliminary sensitivity analyses are performed for stoichiometric iC8/air and iC12/air mixtures at initial conditions of 20 bar and 750 K to understand the reactivity crossover between iC8 and iC12 in the NTC regime, as shown in Figs. 8(a) and 8(b). The molecular structures of important species can be found in Fig. 8(c). As stated earlier, the reactions with positive (negative) sensitivity coefficient tend to inhibit (promote) the overall reactivity.

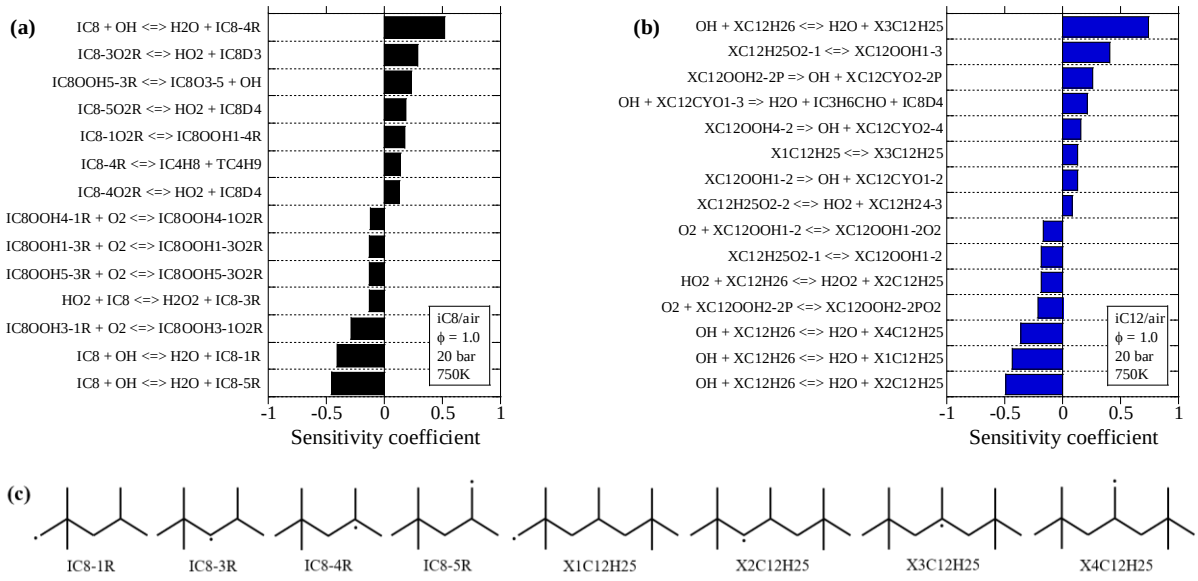

Figure 8: Sensitivity coefficients of important reactions to total ignition delay time at ϕ=1.0, 20 bar, and 750 K for (a) iC8/air and (b) iC12/air. The molecular structures of important species are shown in (c).

For both iC8 and iC12 cases, τ is most sensitive to the rate of ȮH-mediated H-abstraction reactions from fuel molecule. Different fuel H-abstraction paths, however, demonstrate drastically distinct influences of τ. As shown in Figs. 8(a) and 8(b), the production of primary and secondary radicals of fuel (such as IC8-1R and X2C12H25, respectively) is essential in promoting the reactivity of the reacting system. On the other hand, the production of tertiary radicals of fuel (such as IC8-4R and X3C12H25, respectively) is the strongest inhibiting reaction. This is because the tertiary fuel radicals have weaker ability to facilitate low temperature chain branching steps compared to primary and secondary fuel radicals. For iC12 in particular, the overall reaction rate is sensitive to the reaction X1C12H25⟺X3C12H25 in the iC12 sub-model, while the counterpart iC8-1R⟺iC8-4R in the iC8 sub-model is far less important at the condition investigated. This could be one reason that causes the reactivity crossover between iC8 and iC12 in the NTC regime, namely iC12 tends to produce more tertiary fuel radicals (X3C12H25) in the NTC regime and hence suffers more from the resulting inhibiting effect. As a result, iC12 has longer τ than iC8 in the NTC regime. Since other chemical interactions may also play an important role leading to the reactivity crossover, more detailed model-based analyses are needed to understand the reactivity crossover among the *iso*-alkanes studied herein.

5. Conclusions

The autoignition experiments of *iso*-octane (iC8), *iso*-nonane (iC9), and *iso*-dodecane (iC12) in air are performed using a rapid compression machine in this study at varying compressed pressures and equivalence ratios. All three *iso*-alkanes show similar autoignition trend that the total ignition delay time decreases with increasing temperature in the low temperature regime (LTR) and the intermediate temperature regime (ITR) but increases as temperature is increased in the negative temperature coefficient (NTC) regime. The three *iso*-alkanes also demonstrate similar responses to the pressure and equivalence ratio variations; the total ignition delay time decreases with increasing pressure and ϕ. On the other hand, the first-stage ignition delay times are less sensitive to the pressure and ϕ variations, especially in the iC9/air case.

Comparing the newly-acquired iC8/iC9/iC12 data and the literature iC16 data, the four *iso*-alkanes all exhibit NTC response but in different extent, with iC8 showing the strongest NTC response while iC9 displaying the weakest one. In the ITR, the reactivity order is iC9>iC16>iC12>iC8, while iC8 and iC12 have similar total ignition delay times. In the LTR, the total ignition delay times of iC9 and iC12 overlaps well and iC8 shows longer total ignition delay times. Furthermore, the total ignition delay crossovers among iC8/iC12/iC16 are observed in the NTC regime over the conditions investigated. This, in turn, suggests that there are more complicated chemical kinetics involved in the NTC regime for *iso*-alkanes due to their different molecular structures, leading to the observed reactivity crossovers. Comparing the first stage ignition delay times among *iso*-alkanes, a more consistent trend is shown and the first-stage ignition delay order generally follows iC9<iC12<iC8 at all test conditions. Whether iC16 exhibits longer or shorter first-stage ignition delay times requires further investigation by accounting for the heat loss effects in different RCM experiments.

Furthermore, a detailed chemical kinetic model of iC8 and iC12 is developed in this study and validated against the newly-acquired autoignition data. Overall, the current model presents good agreement against experimental data at various test conditions with small discrepancies likely caused by the missing pressure dependency for some reactions. Moreover, the reactivity crossover in the NTC

regime between iC8 and iC12 and the general first-stage ignition delay trend have been successfully captured by the current model. Model-based sensitivity analyses show that one possible reason leading to the reactivity crossover is the different influence of isomerization reaction of primary fuel radical in the iC8 and iC12 sub-mechanisms.

This study provides insights and validation datasets for understanding the fuel molecular structure effect on autoignition characteristics of the selected highly-branched *iso*-alkanes at low-to-intermediate temperatures. Future work will focus on the development of iC9 and iC16 sub-models and involving more different branched-chain alkanes to achieve comprehensive understanding of low temperature combustion of branched hydrocarbons.

Acknowledgements

The work at UCONN was supported by the Lawrence Livermore National Laboratory via Standard Research Subcontract No. B630575 and the National Science Foundation under Grant No. CBET-1402231. The work at LLNL was performed under the auspices of the U.S. Department of Energy (DOE), Contract DE-AC52-07NA27344 and was conducted as part of the Co-Optimization of Fuels & Engines (Co-Optima) project sponsored by the DOE Office of Energy Efficiency and Renewable Energy (EERE), Bioenergy Technologies and Vehicle Technologies Offices.

References

[1] W.J. Pitz, C.J. Mueller, Recent progress in the development of diesel surrogate fuels, Prog. Energy Combust. Sci. 37 (2011), 330-350.

[2] N. Atef, G. Kukkadapu, S.Y. Mohamed, M. Al Rashidi, et al., A comprehensive iso-octane combustion model with improved thermochemistry and chemical kinetics. Combust. Flame (2017) 111-134.

[3] H.S. Shen, J. Vanderover, M.A. Oehlschlaeger, A shock tube study of iso-octane ignition at elevated pressures: the influence of diluent gases, Combust. Flame 155 (2008) 739–755.

[4] S.H. Won, F. M. Haas, A. Tekawade, G. Kosiba et al., Combustion characteristics of C4 iso-alkane oligomers: Experimental characterization of iso-dodecane as a jet fuel surrogate component, Combust. Flame 165 (2016) 137-143.

[5] M. Hartmann, I. Gushterova, M. Fikri, C. Schulz et al., Auto-ignition of toluene-doped n-heptane and iso-octane/air mixtures: High-pressure shock-tube experiments and kinetics modeling, Combust. Flame 158(2011) 172-178.

[6] D. J. Vermeer, J.W. Meyer, A.K. Oppenheim, Auto-ignition of hydrocarbons behind reflected shock waves, Combust. Flame 18(1972) 327-336.

[7] G. Vanhove, R. Minetti, S. Touchard, R. Fournet et al., Experimental and modeling study of the autoignition of 1-hexene/isooctane mixtures at low temperatures, Combust. Flame 145(2006) 272-281.

[8] H.J. Curran, P. Gaffuri, W.J. Pitz, C.K. Westbrook, A comprehensive modeling study of iso-octane oxidation, Combust. Flame 129(2002) 253-280.

[9] D. F. Davidson, M.A. Oehlschiaeger, J.T. Herbon, R.K. Hanson, Shock tube measurements of iso-octane ignition times and OH concentration time histories, Proc. Combust. Inst. 29(2002) 1295-1301.

[10] D.F. Davidson, B.M. Gauthier, R.K. Hanson, Shock tube ignition measurements of iso-octane/air and toluene/air at high pressures, Proc. Combust. Inst. 30 (2005) 1175–1182.

[11] R. Minetti, M. Carlier, M. Ribaucour, E. Therssen et al., Comparison of oxidation and autoignition of the two primary reference fuels by rapid compression, Symp. (Int.) Combust. 26 (1996) 747-753.

[12] K. Fieweger, R. Blumenthal, G. Adomeit, Self-ignition of S.I. engine model fuels: a shock tube investigation at high pressure, Combust. Flame 109 (1997) 599–619.

[13] K. Fieweger, R. Blumenthal, G. Adomeit, Shock-tube investigations on the self-ignition of hydrocarbon-air mixtures at high pressures, Symp. (Int.) Combust. 25 (1994) 1579–1585.

[14] T. Malewicki, A. Comandini, K. Brezinsky, Experimental and modeling study on the pyrolysis and oxidation of iso-octane, Proc. Combust. Inst. 34 (2013) 353–360.

[15] A. Cox, J.F. Griffiths, C. Mohamed, H.J. Curran, W.J. Pitz, C.K. Westbrook, Extents of alkane combustion during rapid compression leading to single-and two-stage ignition, Symp. (Int.) Combust. 26 (1996) 2685–2692.

[16] J.F. Griffiths, P.A. Halford-Maw, D.J. Rose, Fundamental features of hydrocarbon autoignition in a rapid compression machine, Combust. Flame 95 (1993) 291–306.

[17] C.V. Callahan, T.J. Held, F.L. Dryer, R. Minetti et al., Experimental data and kinetic modeling of primary reference fuel mixtures, Symp. (Int.) Combust. 26 (1996) 739–764.

[18] R. Minetti, M. Carlier, M. Ribaucour, E. Therssen, L.R. Sochet, Comparison of oxidation and autoignition of the two primary reference fuels by rapid compression, Symp. (Int.) Combust. 26 (1996) 739–764.

[19] R. Minetti, M. Ribaucour, M. Carlier, L.R. Sochet, Autoignition delays of a series of linear and branched chain alkanes in the intermediate range of temperature, Combust. Sci. Technol. 113 (1996) 747–753.

[20] X. He, M.T. Donovan, B.T. Zigler, T.R. Palmer et al., An experimental and modeling study of iso-octane ignition delay times under homogeneous charge compression ignition conditions, Combust. Flame 142 (2005) 266–275.

[21] X. He, B.T. Zigler, S.M. Walton, M.S. Wooldridge et al., A rapid compression facility study of OH time histories during iso-octane ignition, Combust. Flame 145 (2006) 552–570.

[22] S.M. Walton, X. He, B.T. Zigler, M.S. Wooldridge et al., An experimental investigation of iso-octane ignition phenomena, Combust. Flame 150 (2007) 246–262.

[23] L. Yu et al., A study on the low-to-intermediate temperature ignition delays of long chain branched paraffin: Iso-cetane, Proc. Combust. Inst. (2018), https://doi.org/10.1016/j.proci.2018.08.039 (in press).

[24] G. Kukkadapu, C.J. Sung, Autoignition study of binary blends of n-dodecane/1-methylnaphthalene and iso-cetane/1-methylnaphthalene, Combust. Flame 189 (2018) 367-377.

[25] M.A. Oehlschlaeger, J. Steinberg, C.K. Westbrook, W.J. Pitz, The autoignition of iso-cetane at high to moderate temperatures and elevated pressures: shock tube experiments and kinetic modeling, Combust. Flame 156 (2009) 2165–2172.

[26] P. Dagaut, K. Hadj-Ali, Chemical kinetic study of the oxidation of iso-cetane in a jet stirred reactor: experimental and modeling, Energy Fuels 23 (2009) 2389–2395.

[27] G. Flora, J. Balagurunathan et al., Chemical ignition delay of candidate drop-in replacement jet fuels under fuel-lean conditions: A shock tube study. Fuel, 209 (2017) 457-472.

[28] G. Mittal, C.J. Sung, A rapid compression machine for chemical kinetics studies at elevated pressures and temperatures, Combust. Sci. Tech. 179 (2007) 497-530.

[29] A.K. Das, C.J. Sung, Y. Zhang, G. Mittal, Ignition delay study of moist hydrogen/oxidizer mixtures using a rapid compression machine, Int. J. Hydrogen Energy 37 (2012) 6901-6911.

[30] B.W. Weber, C.J. Sung, UConnRCMPy: Python-Based Data Analysis for Rapid Compression Machines, Proc. the 15th Python in Science Conference (2016) 36-44.

[31] D. Lee, S. Hochgreb, Rapid compression machines: Heat transfer and suppression of corner vortex, Combust. Flame 114 (1998) 531-545.

[32] C.J. Sung, H.J. Curran, Using rapid compression machines for chemical kinetics studies, Prog. Energy Combust. Sci. 44 (2014) 1-18.

[33] R. Fang, G. Kukkadapu, M. Wang et al., Fuel molecular structure effect on autoignition of highly-branched iso-alkanes at low-to-intermediate temperatures, 2019 (in preparation)

[34] K. Zhang, C. Banyon, U. Burke, G. Kukkadapu, S. W. Wagnon, M. Mehl, H. Curran, C. K. Westbrook, W. J. Pitz, An experimental and kinetic modeling study of the oxidation of hexane isomers: developing consistent reaction rate rules for alkanes, Combust. Flame, In review.

[35] Y. Li, C.W. Zhou, K.P. Somers, K. Zhang, and H.J. Curran, The oxidation of 2-butene: A high pressure ignition delay, kinetic modeling study and reactivity comparison with isobutene and 1-butene, Proc. Combust. Inst. 36 (2017) 403–411.

[36] H. J. Curran, P. Gaffuri, W. J. Pitz, C. K. Westbrook, A comprehensive modeling study of iso-octane oxidation, Combust. Flame 129 (2002) 253-280.

[37] M. Mehl, W.J. Pitz, C.K. Westbrook, H.J. Curran, Kinetic modeling of gasoline surrogate components and mixtures under engine conditions, Proc. Combust. Inst. 33 (2011) 193-200.

[38] J. Badra, A. Farooq, Site-specific reaction rate constant measurements for various secondary and tertiary H-abstraction by OH radicals, Combust. Flame 162 (2015) 2034-2044.

[39] A. Miyoshi, Systematic computational study on the unimolecular reactions of Alkylperoxy (RO2), hydroperoxyalkyl (QOOH), and hydroperoxyalkylperoxy (O2QOOH) radicals, J. Phys. Chem. A 115 (2011) 3301-3325.

[40] S.M. Villano, L.K. Huynh, H.H. Carstensen, and A.M. Dean, High-pressure rate rules for alkyl + O2 reactions. 1. The dissociation, concerted elimination, and isomerization channels of the alkyl peroxy radical, J. Phys. Chem. A 115 (2011) 13425-13442.

[41] S.M. Villano, L.K. Huynh, H.H. Carstensen, and A.M. Dean, High-pressure rate rules for alkyl + O2 reactions. 2. The isomerization, cyclic ether formation, and β-scission reactions of hydroperoxy alkyl radicals, J. Phys. Chem. A 116 (2012) 5068-5089.

[42] S. Sharma, S. Raman, W.H. Green, Intramolecular Hydrogen Migration in Alkylperoxy and Hydroperoxyalkylperoxy Radicals: Accurate Treatment of Hindered Rotors, J. Phys. Chem. A 114 (2010) 5689-5701.

[43] S.M. Burke, J.M. Simmie, H.J. Curran, Critical Evaluation of Thermochemical Properties of C1–C4 Species: Updated Group-Contributions to Estimate Thermochemical Properties, J. Physical and Chemical Reference Data 44 (2015) 013101.

[44] D.G. Goodwin, H.K. Moffat, R. L. Speth, Cantera: An object-oriented software toolkit for chemical kinetics, thermodynamics, and transport processes. http://www.cantera.org, (2017) Version 2.3.0.

[45] E.E. Dames, A.S. Rosen, B.W. Weber et al., A Detailed Combined Experimental and Theoretical Study on Dimethyl Ether/Propane Blended Oxidation, Combust. Flame 168 (2016) 310–330.

[46] D.F. Davidson, R.K. Hanson, Recent advances in shock tube/laser diagnostic methods for improved chemical kinetics measurements, Shock Waves 19 (2009) 271-283.

[47] G.A. Pang, D.F. Davidson, R.K. Hanson, Experimental study and modeling of shock tube ignition delay times for hydrogen–oxygen–argon mixtures at low temperatures, Proc. Combust. Inst. 32 (2009) 181-188.

[48] C.K. Westbrook, W.J. Pitz, O. Herbinet, H.J. Curran et al., A comprehensive detailed chemical kinetic reaction mechanism for combustion of n-alkane hydrocarbons from n-octane to n-hexadecane. Combust. Flame, 156 (2009) 181-199.